

PCCP

Accepted Manuscript



This is an *Accepted Manuscript*, which has been through the Royal Society of Chemistry peer review process and has been accepted for publication.

Accepted Manuscripts are published online shortly after acceptance, before technical editing, formatting and proof reading. Using this free service, authors can make their results available to the community, in citable form, before we publish the edited article. We will replace this *Accepted Manuscript* with the edited and formatted *Advance Article* as soon as it is available.

You can find more information about *Accepted Manuscripts* in the [Information for Authors](#).

Please note that technical editing may introduce minor changes to the text and/or graphics, which may alter content. The journal's standard [Terms & Conditions](#) and the [Ethical guidelines](#) still apply. In no event shall the Royal Society of Chemistry be held responsible for any errors or omissions in this *Accepted Manuscript* or any consequences arising from the use of any information it contains.

**PCCP**

Quantum Coherence Effects in Natural Light-Induced Processes: Cis-Trans Photoisomerization of Model Retinal Under Incoherent Excitation

Journal:	<i>Physical Chemistry Chemical Physics</i>
Manuscript ID:	CP-ART-03-2015-001388.R1
Article Type:	Paper
Date Submitted by the Author:	13-May-2015
Complete List of Authors:	Tscherbul, Timur; University of Toronto, Brumer, P; University Toronto, Department of Chemistry

SCHOLARONE™
Manuscripts

Quantum Coherence Effects in Natural Light-Induced Processes: *Cis-Trans* Photoisomerization of Model Retinal Under Incoherent Excitation

Timur V. Tscherbul and Paul Brumer

*Chemical Physics Theory Group, Department of Chemistry,
and Center for Quantum Information and Quantum Control,
University of Toronto, Toronto, Ontario, M5S 3H6, Canada**

(Dated: May 10, 2015)

Abstract

We present a theoretical study of quantum coherence effects in the primary *cis-trans* photoisomerization of retinal in rhodopsin induced by incoherent solar light. Using the partial secular Bloch-Redfield quantum master equation approach based on a two-state two-mode linear vibronic coupling model of the retinal chromophore [S. Hahn and G. Stock, *J. Phys. Chem. B*, 2000, **104**, 1146-1149], we show that a sudden turn-on of incoherent pumping can generate substantial Fano coherences among the excited states of retinal. These coherences are the most pronounced in the regime where the matrix elements of the transition dipole moment between the ground and excited eigenstates are parallel to one another. We show that even when the transition dipole moments are perpendicular (implying the absence of light-induced Fano coherence) a small amount of excited-state coherence is still generated due to the coupling to intramolecular vibrational modes and the protein environment, causing depopulation of the excited eigenstates. The overall effect of the coherences on the steady-state population and on the photoproduct quantum yield is shown to be small; however we observe a significant transient effect on the formation of the *trans* photoproduct, enhancing the photoreaction quantum yield by $\sim 11\%$ at 200 fs. These calculations suggest that coupling to intramolecular vibrational modes and the protein environment play an important role in photoreaction dynamics, suppressing oscillations in the quantum yield associated with Fano interference.

I. INTRODUCTION

The experimental observation of long-lasting wavelike energy transfer in photosynthetic light-harvesting complexes (LHCs)¹⁻⁵ has opened up a fascinating field of research exploring the nature of non-trivial quantum effects (such as coherence and entanglement) in biological processes⁶. In these experiments, sequences of ultrashort, coherent laser pulses are used to initiate and probe excitonic energy transfer in photosynthetic light harvesting^{1,2}, organic photovoltaics⁷, and visual phototransduction⁸. Theoretical analysis of the two-dimensional photon echo signals provides insights into the origin and dynamics of inter-chromophoric energy transfer within the LHCs³⁻⁵. Recent theoretical studies have suggested that quantum coherence and entanglement might play a significant role in the energy transfer process under ambient conditions, enhancing its efficiency via a number of mechanisms, including environment-assisted energy transfer⁹, supertransfer¹⁰, and Fano interference¹¹. Discussions questioning the role of quantum effects have also been advanced^{12,13}

When interpreting the results of ultrafast spectroscopic experiments, it is important to keep in mind that photosynthetic organisms, photovoltaic devices, and rod cells in the retina harvest solar light, which differs from femtosecond laser light in several important respects. First, the coherence time of the solar radiation is many orders of magnitude shorter than that of a fully coherent laser pulse. Quite unlike the latter, solar light is best thought of as a random signal with a very short coherence time (1.3 fs), which is negligible on all timescales of practical interest^{14,15}. Averaging over the different realizations of this noise is expected to rapidly quench quantum interferences¹⁵ and, thus, excitation by solar light should ultimately produce incoherent mixtures of molecular eigenstates, which do not evolve in time^{14,16}. Second, ultrafast laser pulses produce localized excitations, which are time-evolving coherent superpositions of excited eigenstates of the system⁴. The timescale on which natural light harvesting occurs by far exceeds the duration of a femtosecond laser pulse. As a result, in natural systems there is no obvious separation of timescales between incoherent excitation, exciton transport, and their trapping at the reaction center, and all of these processes should be considered simultaneously, thereby complicating theoretical modeling.

The nature of molecular excited states prepared by incoherent solar light has been the subject of many recent theoretical studies^{11,14,17-23}. In particular, Scully and co-workers explored the dynamical and steady-state properties of few-level systems pumped by incoherent radiation using the Bloch-Redfield master equation approach^{11,19-21} and showed that

stationary quantum coherences can arise even under incoherent illumination, and may contribute positively to the efficiency of quantum heat engines and photovoltaic devices. The Fano coherences arise due to quantum interference between the different incoherent excitation pathways^{19,24}. An essential condition for the interference to occur under excitation by isotropic and unpolarized incoherent radiation is non-orthogonality of the transition dipole moments connecting the excited eigenstates to a common ground state^{19,22–24}. The physical manifestation of the Fano coherences depends on the magnitudes of excited-state level splittings and spontaneous decay rates, the details of how the incoherent radiation is turned on, and on whether or not the excited states experience non-radiative decay and decoherence. A proper theoretical description of the Fano coherences requires going beyond the secular approximation, explicitly considering the coupling between the populations and coherences in the eigenstate basis^{11,20–23}.

We have recently shown^{22,23} that the dynamics of the Fano coherences in model few-level systems suddenly exposed to incoherent radiation is determined by the ratio of excited-level splitting to the radiative decay width Δ/γ . If this ratio is large, the excited-state coherences exhibit damped oscillations. In the opposite regime $\Delta/\gamma \ll 1$, we found long-lived quasistationary coherences whose lifetime tends to infinity in the limit $\Delta \rightarrow 0$. These intriguing results call for examination of the possible role of Fano coherences in biologically relevant photoreactions, such as visual phototransduction and excitation energy transfer in photosynthetic light harvesting.

In this article, we explore the role of Fano coherences induced by suddenly turned on incoherent excitation in *cis-trans* photoisomerization of retinal in rhodopsin. This primary photoreaction in vision has a number of exquisite features that made it the focus of numerous experimental and theoretical studies over the last 20 years²⁵. In particular, (1) photoinduced *cis-trans* isomerization occurs in the first 200 fs following impulsive excitation of *cis*-retinal from the ground state²⁶, (2) all-*trans* photoproduct is produced with a high quantum yield of 65 %²⁷, and (3) the protein environment (rhodopsin) enhances the photoreaction quantum efficiency. Several theoretical models have been developed to describe the initial stages of photoinduced *cis-trans* isomerization^{28,29}, among which the two-state, two-mode (TSTM) model of Stock and Hahn²⁸ includes the key torsional and vibronically active modes involved in the isomerization process. This “minimal” model features a conical intersection between the ground and the first excited electronic states of the retinal chromophore, and reproduces the ultrafast timescale of the photoreaction, its high quantum yield, and the qualitative features of its transient absorption spectrum^{30,31}. Recent ultrafast spectroscopic experiments

and time-dependent simulations confirmed the essential role of the conical intersection in determining the subpicosecond timescale of photoisomerization dynamics⁸.

Here, we use the recently developed²³ partial secular Bloch-Redfield (PSBR) quantum master equation approach to describe the excitation of the retinal chromophore (subsystem) by incoherent light treated as a quantum bath of radiation field modes linearly coupled to the subsystem. The Bloch-Redfield quantum master equation is the standard and highly accurate theoretical tool for describing incoherent pumping of few-level quantum optical systems^{24,32,33}. Here, we adapt the PSBR quantum master equation to describe weak-field incoherent optical excitation of retinal in rhodopsin using the TSTM model²⁸⁻³¹. We find that sudden turn-on of incoherent excitation leads to the generation of time-evolving coherences among the excited states of retinal that survive in the steady-state. Remarkably, these Fano coherences can arise not only under incoherent excitation, but also in phonon bath-induced relaxation of excited eigenstates. Hence, the condition of non-orthogonal transition dipole moments required for the generation of coherences in isolated multilevel systems^{11,20,21,23,24} is not necessary for molecular systems embedded in condensed-phase environments.

The calculations reported below show that the effect of Fano coherences on the overall time dynamics of *trans*- photoproduct is weak due to the strong relaxation and decoherence induced by the phonon bath. These coherences do lead to a transient enhancement of the photoreaction quantum yield by as much as 11%, but they play a small role in the long-time limit, where the value of the quantum yield is determined by the system-bath coupling rather than by the transition dipole alignment. Finally, we show that coupling to the phonon bath, apart from inducing detrimental relaxation and decoherence, can also have a positive effect, increasing both the rate of *trans*-product formation and the long-time value of the quantum yield.

In addition to the above results, model calculations with artificially scaled relaxation parameters presented below suggest that the product dynamics is strongly modified by the presence of quantum coherences when the system-bath coupling is weak. In particular, the quantum yield for *cis-trans* isomerization exhibits pronounced oscillations associated with the Fano coherences, which are suppressed by the environment. Our work also suggests that stationary quantum coherences among excited eigenstates in large molecules can form and persist over a long time in the presence of strong environmental dephasing.

This paper is organized as follows. Section II presents the main components of our theoretical model for retinal photoisomerization under incoherent excitation, including the two-state, two-mode model of the retinal chromophore, the associated coupling to a phonon

environment^{28,30,31}, and the PSBR theory of incoherent excitation²³. Section III presents the results for the time evolution of Fano coherences, photoproduct populations, and the photoreaction quantum yield, along with an analysis of the role of quantum coherence in the initial steps of retinal photoisomerization. Section IV summarizes the main results and conclusions, and outlines several possible directions of future work.

II. THEORETICAL MODEL FOR QUANTUM COHERENCES IN RETINAL PHOTOISOMERIZATION

The quantum dynamics of *cis-trans* photoisomerization of the retinal chromophore induced by incoherent light is described by the following equation of motion

$$\frac{d}{dt}\hat{\rho} = -i[\hat{H}_S, \hat{\rho}] + \mathcal{L}_{\text{rad}}[\hat{\rho}] + \mathcal{L}_{\text{ph}}[\hat{\rho}], \quad (1)$$

where the first term on the right-hand side describes the unitary evolution of the system under \hat{H}_S , $\mathcal{L}_{\text{rad}}[\hat{\rho}]$ is the Liouville operator describing the interaction of the system with incoherent radiation (solar light), and $\mathcal{L}_{\text{ph}}[\hat{\rho}]$ describes the effect of the phonon bath comprised of low-frequency vibrational modes of retinal along with the motion of the surrounding protein environment. The reduced density operator $\hat{\rho} = \text{Tr}_{\text{rad}}\text{Tr}_{\text{ph}}\rho_{\text{full}}$, where $\rho_{\text{full}} = |\Psi\rangle\langle\Psi|$ is the full system-plus-baths density matrix, and the traces are taken over the degrees of freedom of the radiation field (Tr_{rad}) and the phonon environment (Tr_{ph}). We note that $\hat{\rho}_{\text{full}}$ evolves in time according to the Liouville-von Neumann equation $\frac{d}{dt}\hat{\rho}_{\text{full}} = -i[\hat{H}, \hat{\rho}_{\text{full}}]$, where

$$\hat{H} = \hat{H}_S + \hat{H}_{S-\text{rad}} + \hat{H}_{S-\text{ph}} + \hat{H}_{\text{rad}} + \hat{H}_{\text{ph}} \quad (2)$$

is the full system-plus-bath Hamiltonian, $\hat{H}_{S-\text{rad}}$ is the system-light interaction and $\hat{H}_{S-\text{ph}}$ accounts for the interactions with molecular degrees of freedom not included in \hat{H}_S . The Hamiltonians of the light (or phonon) baths are given by \hat{H}_{rad} (or \hat{H}_{ph}).

In our case, H_S in Eq. (1) is the two-state two-mode (TSTM) model Hamiltonian of the retinal chromophore^{28,30}

$$\hat{H}_S = \sum_{n,n'} \left[\left(\hat{T} + E_n + (-1)^n \frac{1}{2} \tilde{V}_n (1 - \cos \phi) + \omega x^2 / 2 + \kappa x \delta_{n,1} \right) \delta_{nn'} + \lambda x (1 - \delta_{nn'}) \right] |n\rangle\langle n'| \quad (3)$$

which includes the key degrees of freedom involved in retinal photoisomerization: the low-frequency tuning mode $\phi \in [-\pi/2, 3\pi/2]$ and the high-frequency stretching mode x . As pictured in Fig. 1(a), the range of $\phi \in [-\pi/2, \pi/2]$ corresponds to the *cis*-isomer of retinal

and $\phi \in [\pi/2, 3\pi/2]$ – to the *trans*-isomer. In Eq. (3) \hat{T} is the nuclear kinetic energy, $|n\rangle = \psi_n$ ($n = 0, 1$) are the diabatic electronic states, which give rise to a conical intersection²⁸ at $\phi \sim \pi/2$ and $x = 0$ that plays a crucial role in the isomerization process⁸. The potential energy minimum corresponding to state $|n\rangle$ is given by E_n ($E_0 = 0$), and we use the same TSTM model parameters ω , λ , and \tilde{V}_n as given in Refs. 28,29. It is worth noting that the model in Eq. (3) reproduces many salient features of *cis-trans* photoisomerization dynamics in retinal, including the high quantum yield, the pump-probe absorption spectrum, and the energy storage of the photoreaction^{28–31}. The model is adequate on short time scales, and we use it here to explore the photoreaction dynamics at times up to ~ 2 ps.

The term $\hat{H}_{S\text{-rad}}$ in Eq. (2) describes the interaction of the retinal subsystem with incoherent radiation in the dipole approximation^{23,32,33}

$$\hat{H}_{S\text{-rad}} = -\boldsymbol{\mu} \sum_{\mathbf{k}, \lambda} \left(\frac{\hbar \omega_{\mathbf{k}}}{2\epsilon_0 V} \right)^{1/2} \hat{\epsilon}_{\mathbf{k}\lambda} (\hat{a}_{\mathbf{k}\lambda} - \hat{a}_{\mathbf{k}\lambda}^\dagger) \quad (4)$$

where $\boldsymbol{\mu}$ is the transition dipole moment operator of the retinal subsystem, $\hat{a}_{\mathbf{k}\lambda}$ and $\hat{a}_{\mathbf{k}\lambda}^\dagger$ are the creation and annihilation operators of the electromagnetic fields modes with frequencies $\omega_{\mathbf{k}}$ and polarization vectors $\hat{\epsilon}_{\mathbf{k}\lambda}$, ϵ_0 is the vacuum permittivity, and V is the cavity volume. Following previous theoretical work, we assume that the transition dipole moment is independent of the nuclear coordinates (the Franck-Condon approximation)^{34,35} and set $\mu = 10$ D.

The term $\hat{H}_{S\text{-ph}}$ in Eq. (2) represents the coupling of the system modes \hat{A}_α to those of the phonon bath \hat{B}_α where α enumerates the degrees of freedom explicitly included in \hat{H}_S (ϕ and x) and

$$\hat{H}_{S\text{-ph}} = \sum_{\alpha} \hat{A}_\alpha \hat{B}_\alpha \quad (5)$$

The Hamiltonian of the phonon bath is $\hat{H}_{\text{ph}} = \sum_{\alpha, n} \omega_{\alpha n} b_{\alpha n}^\dagger b_{\alpha n}$ accounts for the intramolecular modes and external environment interacting with (but not explicitly included in) the retinal subsystem^{29–31}. The bath operators in Eq. (5) are $\hat{B}_\alpha = \sum_n \lambda_{\alpha n} (b_{\alpha n} + b_{\alpha n}^\dagger)$, where $\lambda_{\alpha n}$ quantifies the coupling of system mode α to n -th harmonic oscillator of α -th bath. In the TSTM model, the system operators are given by^{30,31} $\hat{A}_\phi = |\psi_1\rangle\langle\psi_1|(1 - \cos\phi)$ and $\hat{A}_x = |\psi_1\rangle\langle\psi_1|x$. The system-bath coupling coefficients $\lambda_{\alpha n}$ define the spectral density of the bath modes, which we assume to be Ohmic, $J_\alpha(\omega) = \eta_\alpha e^{-\omega/\omega_{c\alpha}}$, where η_α is the coupling parameter, and $\omega_{c\alpha}$ is the cutoff frequency for $\alpha = \phi, x$. We use the same values of the parameters η_α and $\omega_{c\alpha}$ as given in Refs. 30,31.

The Liouville superoperator due to the incoherent light-matter interaction may be written²³ in the basis of system eigenstates $|i\rangle$

$$\begin{aligned}
 (\mathcal{L}_{\text{rad}}[\hat{\rho}])_{ij} = & p_{ij}\rho_{gg}(t)\sqrt{r_i r_j} - \frac{1}{2} \sum_k \rho_{kj}(t)p_{ik} (\sqrt{\gamma_i \gamma_k} + \sqrt{r_i r_k}) \\
 & - \frac{1}{2} \sum_k \rho_{ik}(t)p_{jk} (\sqrt{\gamma_j \gamma_k} + \sqrt{r_j r_k})
 \end{aligned} \quad (6)$$

where $\rho_{ij}(t)$ is the reduced density matrix in the energy basis, r_i is the incoherent pumping rates from the ground state $|g\rangle$ into eigenstate $|i\rangle$, and γ_i is the spontaneous decay rate of eigenstate $|i\rangle$ to the ground state. The matrix elements $p_{ij} = \boldsymbol{\mu}_{gi} \cdot \boldsymbol{\mu}_{gj} / (\mu_{gi}\mu_{gj})$ quantify the amount of alignment between the transition dipole moments, and modulate the magnitude of noise-induced Fano coherences under incoherent excitation²³. Here, $\boldsymbol{\mu}_{gi} = \langle g | \hat{\boldsymbol{\mu}} | i \rangle$ is the matrix element of the transition dipole moment operator [Eq. (4)] between the energy eigenstates $|g\rangle$ and $|i\rangle$. Of particular importance is the first term on the right-hand side of Eq. (6), which produces the Fano coherences from the ground state.

The matrix elements p_{ij} can, in principle, be calculated *ab initio* by computing the transition dipole moment surface $\boldsymbol{\mu}(\phi, x)$ and evaluating its matrix elements over the system eigenstates. To our knowledge, no such calculations have been reported for the retinal chromophore. To demonstrate the importance of the orientation of transition dipole moments, we therefore choose to investigate two limiting scenarios: (1) parallel transition dipole moments, *i.e.* $p_{ij} = 1$ for all i, j , and (2) orthogonal transition dipole moments, *i.e.* $p_{ij} = \delta_{ij}$. In the first scenario, a maximum possible amount of Fano coherence is generated since all transition dipole moments are parallel to one another. In the second scenario, no Fano coherence is generated, giving the case of fully incoherent excitation considered before using the rate equations formalism and a simpler one-dimensional model of retinal³⁴.

Eqs. (6) are called the *partial secular* Bloch-Redfield (PSBR) equations. The partial secular approximation neglects the rapidly oscillating one-photon coherences between the ground and excited state manifolds separated by the optical frequency ω_0 while retaining the essential intra-manifold coherences²³.

The main assumptions underlying Eq. (6) are as follows: (1) the light-matter coupling between the subsystem and the radiation field is small compared to the characteristic energy scales of the system, and the coherence time of the incoherent radiation is infinitely short (the Born-Markov approximation). These assumptions are well justified for molecular systems excited by sunlight due to the very short coherence time of blackbody radiation at $T = 5800$ K ($\tau_c = 1.3$ fs, see Refs. 23,36 for details). In addition, we assume that (1) there is

no coupling due to incoherent light between the states within the ground and within the excited-state manifolds, and (2) incoherent excitation occurs from the ground vibronic state of the retinal chromophore. While assumption (1) is valid under very general conditions²³ assumption (2) is consistent with the TSTM model of retinal²⁸ as the first excited vibronic state in the *cis*-well lies 474 cm^{-1} (682 K) above the ground state and has a negligible thermal population at $T = 300 \text{ K}$. Deviations from Markovian behavior occur on short timescales following the turn-on of the excitation ($t < 10\tau_c$) and can be neglected for later times¹⁸.

The Liouville superoperator that accounts for the coupling between the retinal subsystem and the intramolecular vibrational modes (including those of the protein environment) may be written as^{30,31}

$$(\mathcal{L}_{\text{ph}}[\hat{\rho}])_{ij} = \sum_{k,l} \mathcal{R}_{ijkl} \rho_{kl}(t) \quad (7)$$

where the Redfield tensor elements are given by^{30,31,37}

$$\mathcal{R}_{ijkl} = \sum_{\alpha=\phi,x} \left[-\delta_{lj} \sum_r \Gamma_{irrk}^{(+)\alpha} - \delta_{ik} \sum_r \Gamma_{lrrj}^{(-)\alpha} + \Gamma_{ljik}^{(+)\alpha} + \Gamma_{ljik}^{(-)\alpha} \right]. \quad (8)$$

Here, as above, the index α labels the degrees of freedom included in \hat{H}_S (ϕ and x), each of which is coupled to its own independent bath of harmonic oscillators. This separation assumes that the phonon baths coupled to the different degrees of freedom are uncorrelated³⁰. The spectral correlation tensor for α -th bath may be written as³⁷

$$\Gamma_{ljik}^{(+)\alpha} = \frac{1}{2\pi} \langle l | \hat{A}_\alpha | j \rangle \langle i | \hat{A}_\alpha | k \rangle \int_0^\infty d\tau e^{-i\omega_{ik}\tau} \langle \hat{B}_\alpha(\tau) \hat{B}_\alpha \rangle, \quad (9)$$

where the operators \hat{A}_α and \hat{B}_α are the same as in Eq. (5), and $\langle B_{q\alpha}(\tau) B_\alpha \rangle$ is the two-time correlation function of the bath operators in the interaction picture³⁷. In the continuum limit ($\sum_n \rightarrow \int d\omega$), the two-time correlation functions take the generic form^{36,38}

$$\langle B_\alpha(\tau) B_\alpha \rangle = \frac{1}{2\pi} \int_0^\infty d\omega J_\alpha(\omega) [(1 + n(\omega)e^{-i\omega\tau} + n(\omega)e^{i\omega\tau}] \quad (10)$$

where $n(\omega) = [e^{\hbar\omega/kT} - 1]^{-1}$ is the Bose distribution at temperature T and $J_\alpha(\omega) = 2\pi \sum_n \kappa_{\alpha n}^2 \delta(\omega - \omega_n)$ is the spectral density of the bath, which characterizes the strength of the system-bath coupling as a function of frequency. We use an Ohmic parametrization for $J_\alpha(\omega)$ as described above.

Substituting the expressions for the correlation functions from Eq. (10) and evaluating the resulting time and frequency integrals analytically, we find for the real part of the

correlation tensor

$$\Gamma_{ljk}^{(+)\alpha} = \frac{1}{2\pi} A_{lj}^\alpha A_{ik}^\alpha B_{ik}^{(+)\alpha} \quad (11)$$

where $A_{lj}^\alpha = \langle l | \hat{A}_\alpha | j \rangle$ are the matrix elements of the system operators [see Eq. 5] and

$$\begin{aligned} \text{Re}(B_{ik}^{(+)\alpha}) &= \pi J_\alpha(\omega_{ik}) n(\omega_{ik}), & (\omega_{ik} > 0); \\ &= \pi J_\alpha(|\omega_{ik}|) [1 + n(\omega_{ik})], & (\omega_{ik} < 0). \end{aligned} \quad (12)$$

are the coefficients arising from the bath correlation function. We note that while the matrix elements $B_{ik}^{(+)\alpha}$ are complex, here we neglect their imaginary part, which would give (small) Lamb shift corrections to the transition energies due to the interaction with the phonon bath.

The two-bath Redfield master equation in the eigenstate basis (7) was used previously by Stock and co-workers³⁰ to study the role of conical intersections in *cis-trans* isomerization of retinal induced by impulsive Franck-Condon excitation. Here we extend this model to study the photoisomerization dynamics *under incoherent excitation* using our recently developed PSBR approach to evaluate the Liouville superoperator $\mathcal{L}_{\text{rad}}[\hat{\rho}]$ ²³. The explicit inclusion of incoherent pumping effects using $\mathcal{L}_{\text{rad}}[\hat{\rho}]$ is an essential new aspect of the present work that allows us to explore the interplay between incoherent excitation and bath-induced relaxation. We note that this work also represents a significant improvement over our previous theoretical study³⁴, which used a simplified one-dimensional model of retinal without a conical intersection, and adopted the secular approximation ($p_{ij} = \delta_{ij}$), which suppressed the Fano coherences.

Numerical integration of the PSBR master equations (1), (6), and (7) (see the Appendix for details) yields the time-evolving density matrix of the retinal subsystem $\rho_{ij}(t)$. The observable properties of the photoreaction such as the populations of the individual *cis* and *trans*-states^{28,30,31} $P_\alpha^{(n)}$ are evaluated from the excited-state density matrix as

$$P_\alpha^{(n)}(t) = \text{Tr}\{\hat{\rho}(t)\hat{P}_\alpha^{(n)}\}. \quad (13)$$

where $\alpha = cis$ or $\alpha = trans$, and $\hat{P}_{\text{cis}}^{(0)} = \Theta(\pi/2 - |\phi|) |\psi_0\rangle\langle\psi_0|$ and $\hat{P}_{\text{trans}}^{(1)} = \Theta(|\phi| - \pi/2) |\psi_1\rangle\langle\psi_1|$ are the projection operators, which divide the full range of the isomerization coordinate into the *cis* and *trans*-regions corresponding to $\phi \in [-\pi/2, \pi/2]$ and $\phi \in [\pi/2, 3\pi/2]$ respectively, as illustrated in Fig. 1. Further, $\Theta(x)$ is the Heaviside step function, and the operators $|\psi_n\rangle\langle\psi_n|$ project onto the ground and excited diabatic electronic states $|\psi_0\rangle$ and $|\psi_1\rangle$. An important quantity that characterizes photoreaction efficiency is the quantum yield defined

as the fraction of the *trans*-product population relative to the overall excited-state population.

$$Y(t) = \frac{P_{\text{trans}}^{(1)}(t)}{P_{\text{cis}}^{(0)}(t) + P_{\text{trans}}^{(1)}(t)}. \quad (14)$$

When evaluating the populations in Eq. (14), we exclude the ground state contribution $\rho_{gg}(t)\langle g|\hat{P}_\alpha^{(n)}|g\rangle$ from Eq. (13). This is necessary to ensure consistency with the previously adopted definition of the quantum yield²⁸, which included only the excited eigenstates populated after impulsive Franck-Condon excitation from the ground state (*i.e.* $\rho_{gg} = 0$ at $t > 0$). Under weak-field incoherent excitation, most of the population remains in the ground state at all times, (*i.e.* $\rho_{gg} \approx 1$ at $t > 0$), hence the need for the correction.

III. RESULTS AND DISCUSSION

Figure 1 encapsulates the key elements of the theoretical framework for incoherent photoexcitation of retinal in rhodopsin formulated above. The TSTM model of the retinal chromophore defines the system eigenvalues ϵ_i shown in Fig. 1 by horizontal lines. The eigenstates $|i\rangle$ can be classified into three categories³⁹: (1) bright eigenstates (*e.g.* $|508\rangle$ and $|512\rangle$) with non-zero oscillator strengths populated in absorption from the ground state; (2) intermediate eigenstates (*e.g.* $|422\rangle$ and $|423\rangle$) populated in relaxation of the bright states, and (3) product states (*e.g.* $|171\rangle$ and $|179\rangle$), which form the steady-state distribution in the long-time limit. We have recently analyzed the spatial localization properties and the relaxation dynamics of the eigenstates in the framework of coherence-free rate equations³⁹. We found, *e.g.*, that while the bright eigenstates are delocalized over the entire range of ϕ , the intermediate and, especially, the product eigenstates are strongly localized in their respective *cis* and *trans*-potential wells³⁹. Below we explore the dynamics of populations and coherences among the bright, intermediate, and product eigenstates, along with the overall properties of the photoreaction, such as the populations $P_{\text{cis}}^{(0)}$, $P_{\text{trans}}^{(1)}$, and the quantum yield (14).

Figure 2(a) shows examples of the time evolution of excited-state populations and coherences following a sudden turn-on of incoherent excitation at $t = 0$. The populations of the bright eigenstates $|508\rangle$ and $|512\rangle$ grow in magnitude before approaching (non-equilibrium) steady-state values within the first 1 ps. The steady-state populations are determined by the interplay between incoherent pumping (r_i in Eq. (6), upward arrows in Fig. 1) and thermal bath-induced relaxation to dark states (\mathcal{R}_{ijkl} in Eq. (7), downward arrows in Fig. 1). Because the phonon bath-induced relaxation is much faster than incoherent pumping, the

steady-state values of excited-state populations are small, as expected for weak-field incoherent excitation. We note that for simplicity we set the values of the pumping rates in Eq. (6) to $r_i = \bar{n}\gamma_i$, where \bar{n} is the equilibrium occupation number of the photon mode with frequency ω , $\bar{n} = (e^{\beta\omega} - 1)^{-1} \sim 3.8 \times 10^{-3}$ for $\omega = 2.8$ eV, the highest-energy state included in our calculations. Natural sunlight excitation corresponds, however, to much lower effective occupation numbers $C\bar{n}$ with $C = 10^{-9} - 10^{-5}$ being a constant factor related to the luminance of the light source³⁴. Because the eigenstate populations and coherences scale linearly with r_i (or C) in the weak-pump limit²², the excited-state density matrix elements calculated for $C = 1$ can be generalized to any value of $C < 1$ by a simple rescaling (provided we remain in the weak-pump limit, $r_i/\gamma_i \ll 1$).

The coherence between the two bright eigenstates $|508\rangle$ and $|512\rangle$ that dominate the isolated TSTM absorption spectrum^{29,39} increases to a maximum value in the first 200 fs before approaching a steady state. It is worth noting that the short-time dynamics of the *trans*-photoproduct for $p_{ij} = 1$ is remarkably similar to that induced by a fully coherent laser pulse^{30,31}.

As shown in Fig. 2, changing the off-diagonal elements of p_{ij} from zero to unity leads to a dramatic increase of bright- and intermediate- and steady-state coherences, which points to the alignment of transition dipole moments as another key determinant of the transient and steady-state behavior of the coherences. This is consistent with previous theoretical work on simple models, which found that the absence of transition dipole alignment ($p_{ij} = \delta_{ij}$) precludes interference among the different incoherent excitation pathways in an isolated atomic or molecular system^{19,22,24}. Thus, excitation by incoherent light of a multilevel system with $p_{ij} = \delta_{ij}$ is expected to produce no coherences. We stress that this conclusion rests upon the reliability of the Born-Markov approximation made in the derivation of the PSBR equations.

We note that a small but non-negligible amount of coherence is evidently present in all panels of Fig. 2. These coherences can be attributed to the effects of the cold phonon bath, representing the intramolecular degrees of freedom and those of the protein environment. It is known that interaction with a noisy environment can generate coherences in the system even if none are present originally, provided the decay occurs to the eigenstates with non-orthogonal transition dipole moments. These coherences are known as spontaneously generated coherences (SGC) in the quantum optical literature^{24,40} and were observed experimentally in quantum dots⁴¹. As shown in Fig. 2, the magnitude of the phonon bath-induced SGC is very small for the bright and product eigenstates considered here, but is more sub-

stantial for the intermediate states plotted in Fig. 2(b). This observation suggests that in a system interacting with an environment and irradiated with incoherent light, the condition $p_{ij} \neq \delta_{ij}$ is not required for the Fano coherences to occur. This is similar to one-photon phase control, which is forbidden in isolated atomic and molecular systems but can become allowed in the presence of an environment^{42–44}.

At very long times, a steady-state distribution is formed and product-state populations increase linearly with time as shown in Fig. 2(c). The transition dipole alignment does not have any effect on product-state populations at short times. Interestingly, in the absence of Fano coherence, the product formation rate $\dot{\rho}_{171,171}$ increases faster than in the presence of the coherence at long times approaching 1 ps. While the coherences among the product eigenstates are negligible in magnitude compared to the populations at $t > 0.5$ ps, they exhibit small oscillations that develop at $t \sim 0.5$ ps and persist at longer times [see the inset of Fig. 2(c)]. We attribute the origin of these oscillations to a cooperative interplay between incoherent pumping and environmental relaxation and decoherence of bright eigenstates.

Figure 3(a) shows the time evolution of the *cis* and *trans*-photoproduct populations under incoherent excitation. The populations follow a linear behaviour at later times, and exhibit slight non-linearities at shorter times. The *trans*-photoproduct population is larger than that of the *cis*-isomer at all times. Changing the orientation of transition dipole moments from parallel (full lines) to orthogonal (dashed lines) affects the overall populations only weakly. As shown in Fig. 3, the Fano coherence enhances the *trans*-population $P_{\text{trans}}^{(1)}(t)$ at short times (up to ~ 200 ps) but suppresses it at longer times. Because the production of the *cis*-isomer is suppressed by Fano interference at all times, the (time-dependent) quantum yield of the photoreaction (14) increases by 5-10% at short times, an effect directly attributable to the Fano interference as discussed below (see also Fig. 5).

The origin of the weak effect of Fano interference on photoproduct populations observed in Fig. 3 could be related to the strong coupling to the phonon bath, which diminishes the effects of the coherences generated by incoherent driving. To explore this hypothesis, we multiply the system-bath couplings η_α (See Sec. II above) by a constant factor $\lambda < 1$. The scaling procedure slows down relaxation and decoherence by a factor of λ^2 , weakening the effect of the phonon bath on the excited eigenstates. In Fig. 4(a) we compare the results for the population and coherence for $\lambda = 1$ and $\lambda = 0.1$. The weakening of the system-bath interaction has a dramatic effect on both the populations and coherences. The $\lambda = 0.1$ populations grow much faster than the $\lambda = 1$ ones, and the coherences show underdamped oscillations. The oscillating behavior of the coherences in Fig. 4(a) is similar

to that predicted elsewhere to occur in the regime $\Delta/\gamma \gg 1$. The latter limit is relevant in the absence of environmental decoherence^{17,18}, in which case $\gamma_d = 0$. However, due to the presence of an external environment in our TSTM retinal calculation, the proper limit to consider here is $\Delta/\gamma_d \gg 1$ rather than $\Delta/\gamma \gg 1$. We note that even for $\lambda = 0.1$, we are still in the regime where $\gamma_{ij}^d \gg \gamma_i, \gamma_j$, so radiative decay of the eigenstates can be neglected and the decoherence timescale is given by $1/\gamma_{ij}^d$ (Ref. 22). Here, γ_{ij}^d is the dephasing rate of ρ_{ij} caused by the interaction of the excited eigenstates with intramolecular environment ($\gamma_d = \gamma_{12}$ for a V-type system with two excited eigenstates $|1\rangle$ and $|2\rangle$). For the TSTM model considered here, γ_d is on the order of $10^3 - 10^4 \gamma_i$, where γ_i is the spontaneous decay rate of eigenstate $|i\rangle$ ($\gamma_i \sim 10$ -100 MHz for bright eigenstates, e.g. $\gamma_{512} = 46$ MHz).

Figure 4(b) illustrates the effects of coupling to the bath on *cis* and *trans* photoproduct populations. The weaker coupling to the bath ($\lambda = 0.1$) slows down the formation of both *cis* and *trans* photoproducts. At the same time, the effects of Fano interference become more pronounced: At $t = 600$ fs, decreasing λ to 0.1 suppresses the amount of *cis*-population by as much as 20% at $t = 500$ fs, leading to a 4% enhancement of the quantum yield as shown in Fig. 5. However, at later times the *trans*-population is suppressed by the Fano interference to the same extent as the *cis*-population, and the quantum yield drops below the value in the absence of Fano interference shown by the horizontal line in Fig. 5.

As shown in Fig. 5, the quantum yield displays short-time oscillations for the realistic system-bath coupling ($\lambda = 1$), and long-time oscillations persisting up to 3 ps for $\lambda = 0.1$. The realistic system-bath interaction thus leads to the disappearance of the Fano coherences between the excited eigenstates induced by incoherent driving, with the decoherence lifetime on the order of 200 fs, comparable to the reaction time^{8,28}. The overall variation of the quantum yield is the largest ($\sim 11\%$) for the TSTM model with parallel transition dipole moments ($p_{ij} = 1$) and weak excited-state decoherence ($\lambda = 0.1$), where the effect of the environment is weak up until $t \sim 200$ fs, and gradually becomes stronger at later times.

The time variation of the quantum yield in the case of orthogonal transition dipole moments (no Fano coherence) does not display any oscillations at short times, regardless of the magnitude of the system-bath coupling. Indeed, in this regime and in the absence of an external environment, the quantum yield is expected to display no time dynamics³⁹. This is consistent with the nearly horizontal line in Fig. 5 (the small downward slope comes from the weak system-bath coupling, $\lambda = 0.1$). The slow monotonic increase of the quantum yield shown by the dashed line in Fig. 5 for $p_{ij} = \delta_{ij}$ and $\lambda = 1$ is therefore due to the Fano coherences arising from the bath-induced decay of (incoherently) populated bright eigenstates.

This illustrates the important point that *in the presence of an external environment, the alignment of transition dipole moments is not required to generate the Fano coherences*. A recent theoretical study²¹ showed that these “partial coherences” may contribute to enhanced efficiency of quantum heat engines.

The steady-state value of the quantum yield in the limit $t \rightarrow \infty$ is an important characteristic of the photoreaction under incoherent excitation. Fig. 5 shows that the asymptotic quantum yield is determined by two factors: (i) the strength of the system-bath coupling, and (ii) the orientation of transition dipole moments. The system-bath coupling has a more dramatic effect, increasing the quantum yield by $\sim 4\%$ when λ is increased from 0.1 to 1, whereas the variation of transition dipole alignment changes Y by $\sim 1\%$. We note that here, as in the discussion of Fig. 4 above, the system-bath coupling has a positive effect on the asymptotic quantum yield. The Fano coherence leads to long-time oscillatory behavior of $Y(t)$ for weak system-bath coupling, but the oscillations will finally converge to the incoherent result (the black line in Fig. 5) as the Fano coherences become suppressed by the populations.

We conclude that while noise-induced Fano coherences have a moderate enhancing effect on the quantum yield in the transient regime (at $t \sim 200$ fs), the asymptotic steady-state value of the quantum yield is determined to a large extent by the system-bath coupling, and is insensitive to these coherences.

IV. SUMMARY AND CONCLUSIONS

We have presented a theoretical model of *cis-trans* photoisomerization of retinal induced by incoherent irradiation with solar light. The model is based on the TSTM model of the retinal chromophore, which incorporates key tuning, coupling, and vibrational modes weakly coupled to a dissipative bath representing the intramolecular degrees of freedom and the protein environment^{28,29}. The interaction with incoherent light is described in the framework of PSBR master equations²³, which are a convenient theoretical tool to study incoherent excitation and phonon-bath-induced relaxation and decoherence in multilevel quantum systems.

Numerical solution of the PSBR equations for the TSTM model provides insight into the role of quantum effects in the primary *cis-trans* photoisomerization of retinal in rhodopsin. We find that incoherent pumping to bright eigenstates generates substantial Fano coherences provided that the transition dipole moments in the energy basis are parallel to one another

(Fig. 2). We also find that interaction with the environment, apart from inducing relaxation and decoherence of the bright states, can create coherences among the intermediate and product eigenstates involved in relaxation. The overall effect of these coherences on photoreaction observables such as the *trans*-product population and quantum yield is small and short-lived. The noise-induced origin of these coherences is nevertheless of interest for such coherences may potentially affect other biological processes, such as photosynthetic light-harvesting¹¹.

The results presented in this work are obtained assuming that incoherent radiation is turned on suddenly and then kept on at a steady value (as manifested by the constant values of the pumping rates r_i in Eq. 6). By contrast, in naturally occurring visual phototransduction and solar light-harvesting processes, the turn-on is often smooth or even adiabatic compared to any molecular timescales. Preliminary calculations⁴⁵ suggest that the coherences shown in Figs. 2-3 survive adiabatic turn-on; however, their time dynamics is often modified. Most importantly, the long-time values of the populations and coherences remain the same irrespective of whether the radiation is turned on suddenly or adiabatically⁴⁵. It is therefore not the sudden turn-on of incoherent radiation that is responsible for the Fano coherences. Rather, as remarked above, these coherences arise as a result of population-to-coherence coupling associated with the invalidity of the secular approximation, and require non-orthogonality of transition dipole moments in the eigenstate basis^{19,22-24}.

The theoretical framework developed in this paper can be applied to study the quantum dynamics of incoherent light-induced energy transfer in biomolecules (such as photosynthetic dimers and the Fenna-Matthew-Olson and PC645 light-harvesting complexes), and multilevel models of quantum heat engines. Such theoretical studies will further elucidate the role of quantum coherence in biological systems under incoherent light illumination, and may help uncover novel ways to improve the efficiency of photovoltaic devices based on Fano coherence, *e.g.* by taking advantage of the multilevel structure of the excited states. Work in these directions is currently in progress.

ACKNOWLEDGEMENTS

This work was supported by the Natural Science and Engineering Council of Canada and the U.S. Air Force Office of Scientific Research under contract number FA9550-13-1-0005.

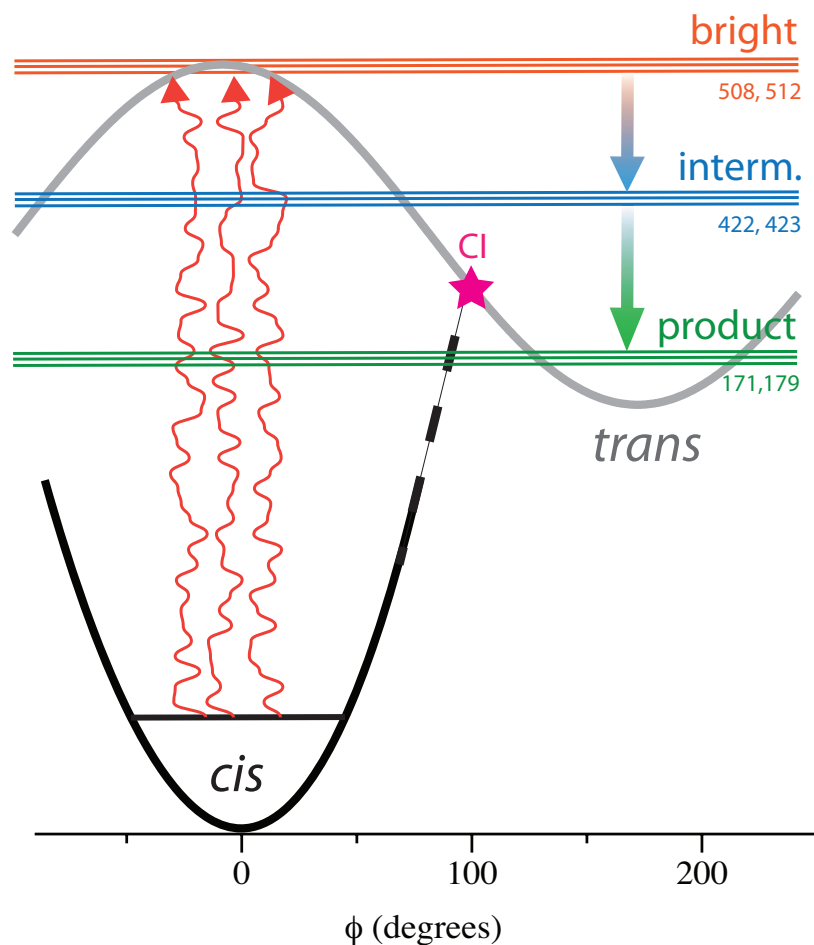


FIG. 1. Quantum dynamics of *cis-trans* photoisomerization in retinal under incoherent light illumination. The ground and excited-state diabatic potentials are shown as curved lines; the eigenstates of the TSTM model obtained by diagonalization of the system Hamiltonian are shown by horizontal lines and classified into bright eigenstates (top, labeled “bright”), intermediate eigenstates participating in bath-induced relaxation (labeled “interm.”), and the eigenstates populated in the long-time limit (green, labeled “product”). The conical intersection is noted as CI. The numbering refers to sample states in these manifolds selected for the calculations shown in Fig. 2.

APPENDIX: COMPUTATIONAL DETAILS

Here we outline the procedure of setting up and solving the PSBR master equations for the retinal system weakly illuminated by incoherent light. The numerical procedure is conveniently separated in three steps: (i) solving for the eigenstates of the TSTM model; (2) evaluating the various terms that parametrize the PSBR equations; and (3) time propagation of the equations.

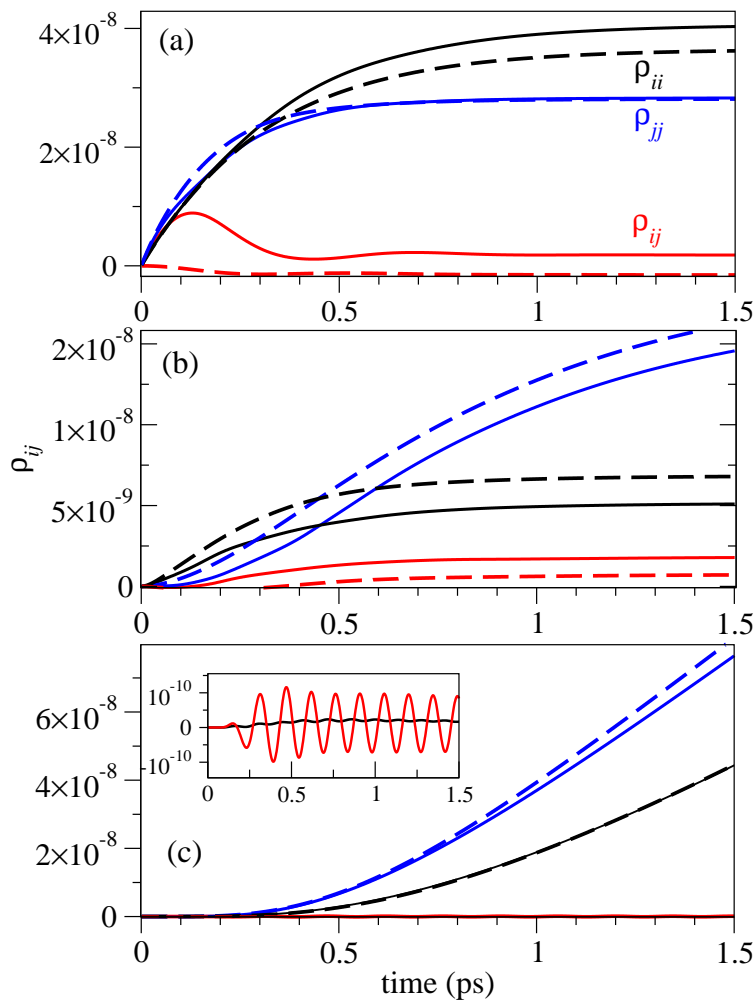


FIG. 2. Time evolution of eigenstate populations and coherences ρ_{ii} , ρ_{jj} (uppermost traces) and $\text{Re}(\rho_{ij})$ (lowermost traces) for the bright eigenstates $i = 508$, $j = 512$ (a), intermediate eigenstates $i = 422$, $j = 423$ (b), and product eigenstates $i = 171$, $j = 179$ (c). The inset in panel (c) shows the real part of the coherence between the product eigenstates $|171\rangle$ and $|179\rangle$. Full lines – parallel transition dipole moments; dashed lines – orthogonal transition dipole moments.

Diagonalization of the system Hamiltonian: First, we obtain the eigenvalue spectrum of the TSTM model (3) which is required to evaluate the Redfield tensor elements \mathcal{R}_{ijkl} in Eq. (8) and the incoherent pumping rates r_i in Eq. (6). To this end, we expand the eigenstates $|i\rangle$ in a direct-product basis

$$|i\rangle = \sum_{n_e, \mu, \nu} C_{i, n_e \mu \nu} \psi_{n_e}(\mathbf{r}_e) \Phi_{\mu}^{n_e}(\phi) X_{\nu}^{n_e}(x) \quad (15)$$

where $\psi_{n_e}(\mathbf{r}_e)$ are the diabatic electronic basis functions, $\Phi_{\mu}^{n_e}(\phi)$ are the (contracted) torsional basis functions and $X_{\nu}^{n_e}(x)$ are the basis functions for the coupling mode (see below).

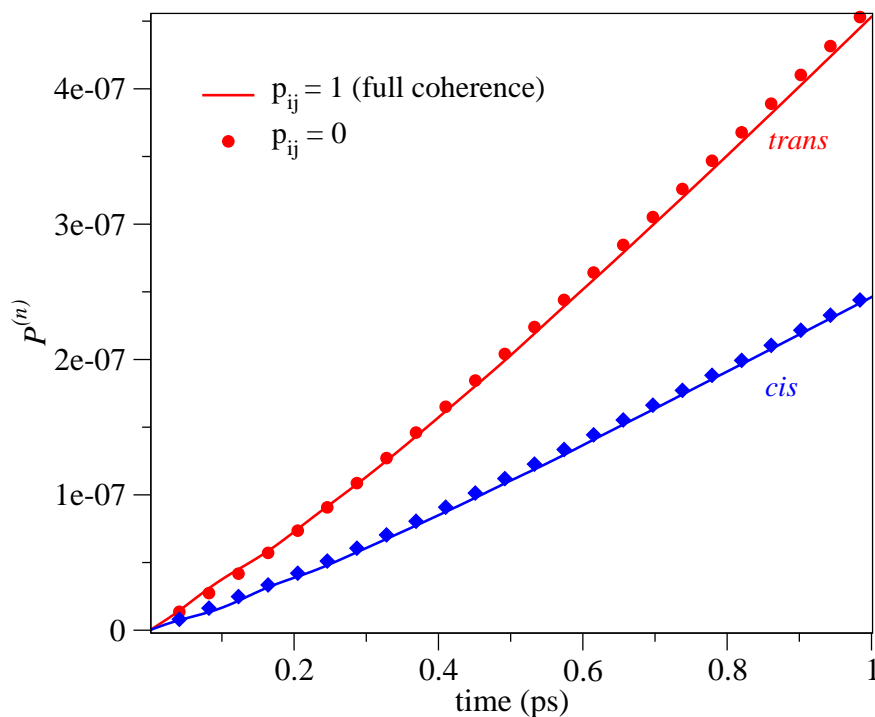


FIG. 3. Time evolution of *cis* and *trans* photoproduct populations: Parallel transition dipole moments (full lines), orthogonal transition dipole moments (symbols).

It is clear from Eq. (3) that in the absence of diabatic coupling between the electronic states ($\lambda = 0$), the Hamiltonian in Eq. (3) becomes separable. We choose the basis functions in Eq. (15) to be the eigenfunctions of the system Hamiltonian (3) at $\lambda = 0$. This choice accelerates numerical convergence of the expansion (15) and is thus preferable over direct expansion in primitive basis functions³⁰.

The contracted basis functions in Eq. (15) are defined as

$$\begin{aligned} \left[-\frac{1}{2m} \frac{\partial^2}{\partial x^2} + \omega x^2/2 + \kappa x \delta_{n_e,1} \right] X_\nu^{n_e}(x) &= \epsilon_\mu^{n_e} X_\mu^{n_e}(x) \\ \left[-\frac{1}{2I} \frac{\partial^2}{\partial \phi^2} + (-1)^{n_e} \frac{1}{2} \tilde{V}_{n_e} (1 - \cos \phi) \right] \Phi_\mu^{n_e}(\phi) &= \epsilon_\mu^{n_e} \Phi_\mu^{n_e}(\phi) \end{aligned} \quad (16)$$

The solutions to these equations were expanded in 200 primitive torsional functions of ϕ obeying periodic boundary conditions⁴⁶, and in 100 particle-in-a-box basis functions of x . The inversion parity of the torsional wavefunctions was set to +1 in all calculations. The coefficients $C_{i,n_e\mu\nu}$ were obtained by diagonalizing the Hamiltonian matrix (3) in the basis of contracted functions (16). The evaluation of the matrix elements is straightforward due to our choice of the basis functions: only the matrix elements of the off-diagonal vibronic coupling need to be computed (and these matrix elements are diagonal in μ since the coupling

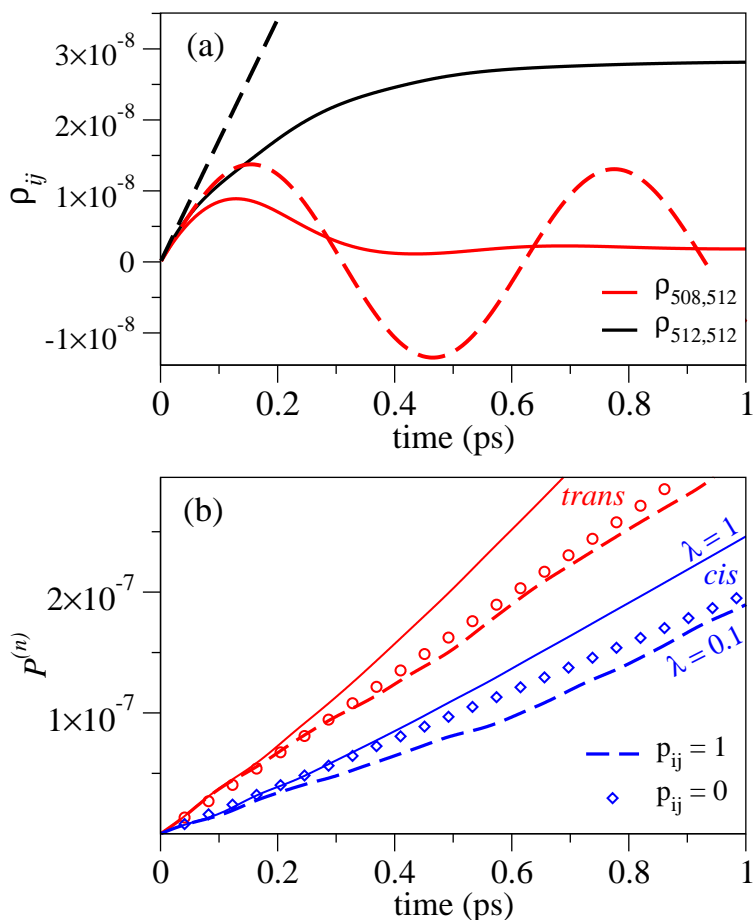


FIG. 4. (a) Populations and coherences between the bright eigenstates for unscaled (full lines) and scaled ($\lambda = 0.1$, dashed lines) system-bath coupling. (b) *cis* and *trans* photoproduct populations for unscaled (full lines) and scaled (dashed lines and symbols) system-bath coupling. Dashed lines – parallel transition dipole moments, symbols – orthogonal transition dipole moments.

in independent of ϕ). A total of 2000 basis functions with $n_e = 0, 1$, $\mu = 0, \dots, 100$, and $\nu = 0, \dots, 20$ were used to assemble the Hamiltonian matrix, whose diagonalization yields the lowest 500 eigenstates converged to within 3-4 significant digits. The eigenstates are then used as a basis to express the system density matrix and calculate the rates of incoherent pumping, spontaneous decay, and phonon-induced relaxation and decoherence.

Solution of PSBR equations: The key computational challenge in solving the PSBR master Eqs. (1), (6), and (7) arises from the need to evaluate the effect of the Redfield tensor on the density matrix. Direct evaluation of Eq. (7) scales as N^4 with the number of system eigenstates N , and becomes computationally challenging already for small N ($\sim 100 - 1000$). In order to make the calculations more efficient, we use the algorithm of

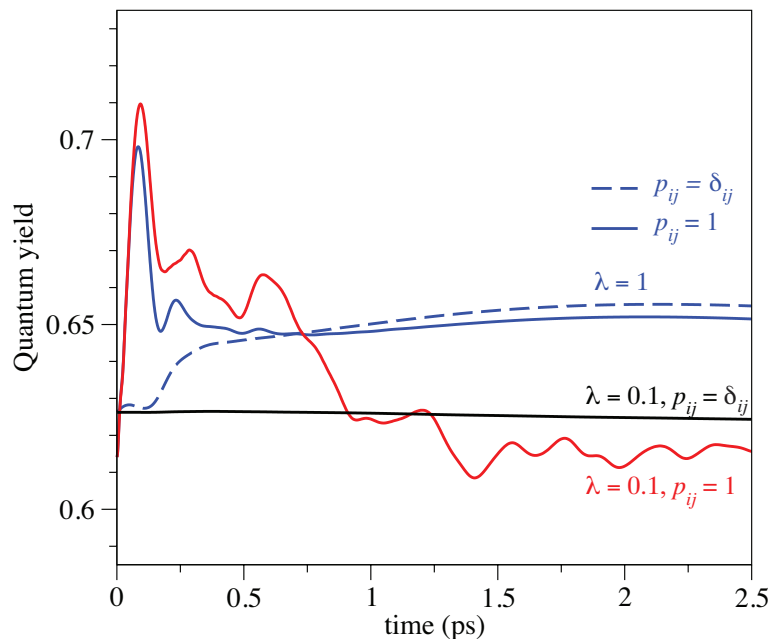


FIG. 5. Time evolution of the photoreaction quantum yield calculated for $\lambda = 1$ and 0.1 , and for parallel and orthogonal transition dipole moments ($p_{ij} = \delta_{ij}$ vs. 1). Each curve is marked by the corresponding values of λ and p_{ij} .

Pollard and Friesner⁴⁷ which takes advantage of the separable structure of Γ_{ijkl}^+ to evaluate the right-hand side of Eq. (7)

$$\mathcal{R}\rho = -M^{(+)}\rho - \rho M^{(-)} + \sum_{\alpha=\phi,x} (P^{(+)\alpha}\rho A^\alpha + A^\alpha\rho P^{(-)\alpha}) \quad (17)$$

where

$$M^{(+)} = \sum_{\alpha} A^\alpha P^{(+)\alpha}, \quad M^{(-)} = \sum_{\alpha} P^{(-)\alpha} A^\alpha, \quad (18)$$

are square $N \times N$ matrices and

$$P_{ik}^{(\pm)\alpha} = \frac{1}{2\pi} A_{ik}^\alpha B_{ik}^{(\pm)\alpha}. \quad (19)$$

with $B_{ik}^{(\pm)\alpha}$ given by Eq. (12). The Pollard-Friesner algorithm scales more favorably as $\sim N^3$ and allows for a more efficient numerical solution of Eqs. (17). The matrix elements A_{ik}^α were evaluated by quadrature integration of system operators over the system eigenstates. The matrices \mathbf{A} and \mathbf{P}^\pm were evaluated once and stored for subsequent use. A total of

500 eigenstates were included in numerical simulations of dissipative dynamics of the TSTM model of retinal induced by incoherent light. The incoherent pumping and spontaneous decay rates were evaluated using standard expressions^{23,33} and the photon occupation number was set to the value $\bar{n} = 3.8 \times 10^{-3}$ appropriate for sunlight radiation at $\omega = 2.8$ eV. Only a small fraction (~ 30 out of 500) of TSTM model eigenstates have non-negligible oscillator strengths with the ground state; these are called the “bright eigenstates” in the main text.

The PSBR equations (1), (6), and (7) were integrated on an equidistant time grid with a step size of 1 fs using the 4-th order Runge-Kutta method. The convergence of our numerical results was verified by reducing the integration time step, and by comparing the results with the analytical expressions for few-level systems derived previously^{22,23}. As a further consistency check, we compared the time variation of photoproduct populations $P_{\text{cis}}^{(1)}(t)$ and $P_{\text{trans}}^{(1)}(t)$ following impulsive Franck-Condon excitation from the ground state with the previous results of Balzer and Stock³¹ and found good qualitative agreement.

* ttscherb@chem.utoronto.ca

- ¹ G. S. Engel, T. R. Calhoun, E. L. Read, T. K. Ahn, T. Mañcal, Y. C. Cheng, R. E. Blankenship and G. R. Fleming, *Nature*, 2007, **446**, 782–786.
- ² E. Collini, C. Y. Wong, K. E. Wilk, P. M. G. Curmi, P. Brumer and G. D. Scholes, *Nature*, 2010, **463**, 644–647.
- ³ L. A. Pachón and P. Brumer, *Phys. Chem. Chem. Phys.*, 2012, **14**, 10094–10108.
- ⁴ Y. C. Cheng and G. R. Fleming, *Annu. Rev. Phys. Chem.*, 2009, **60**, 241–262.
- ⁵ A. Chenu and G. D. Scholes, *Annu. Rev. Phys. Chem.*, 2015, **66**, March 31.
- ⁶ N. Lambert, Y.-N. Chen, Y.-C. Cheng, C.-M. Li, G.-Y. Chen and F. Nori, *Nature Physics*, 2013, **9**, 10–18.
- ⁷ L. G. Kaake, C. Zhong, J. A. Love, I. Nagao, G. C. Bazan, T.-Q. Nguyen, F. Huang, Y. Cao, D. Moses and A. J. Heeger, *J. Phys. Chem. Lett.*, 2014, **5**, 2000–2006.
- ⁸ D. Polli, P. Altoe, O. Weingart, K. M. Spillane, C. Manzoni, D. Brida, G. Tomasello, G. Orlandi, P. Kukura, R. A. Mathies, M. Garavelli and G. Cerullo, *Nature*, 2010, **467**, 440–443.
- ⁹ A. W. Chin, A. Datta, F. Caruso, S. F. Huelga and M. B. Plenio, *New J. Phys.*, 2010, **12**, 065002.
- ¹⁰ S. Lloyd and M. Mohseni, *New J. Phys.*, 2010, **12**, 075020.
- ¹¹ K. E. Dorfman, D. V. Voronine, S. Mukamel and M. O. Scully, *Proc. Natl. Acad. Sci. USA*,

- 2013, **110**, 2746–2751.
- ¹² W. H. Miller, *J. Chem. Phys.*, 2012, **136**, 210901–1–210901–6.
- ¹³ S. Duque, L. A. Pachón and P. Brumer, *arXiv:1412.8743*, 2014.
- ¹⁴ P. Brumer and M. Shapiro, *Proc. Natl. Acad. Sci. USA*, 2012, **127**, 19575–19578.
- ¹⁵ I. Kassal, J. Yuen-Zhou and S. Rahimi-Keshari, *J. Phys. Chem. Lett.*, 2013, **4**, 362–367.
- ¹⁶ X.-P. Jiang and P. Brumer, *J. Chem. Phys.*, 1991, **94**, 5833–5843.
- ¹⁷ Z. S. Sadeq and P. Brumer, *J. Chem. Phys.*, 2014, **140**, 074104.
- ¹⁸ T. V. Tscherbul and P. Brumer, *Phys. Rev. A*, 2014, **89**, 013423–1–013423–8.
- ¹⁹ V. V. Kozlov, Y. Rostovtsev and M. O. Scully, *Phys. Rev. A*, 2006, **74**, 063829–1–063829–10.
- ²⁰ M. O. Scully, K. R. Chapin, K. E. Dorfman, M. B. Kim and A. Svidzinsky, *Proc. Natl. Acad. Sci. USA*, 2011, **108**, 15097–15101.
- ²¹ A. A. Svidzinsky, K. E. Dorfman and M. O. Scully, *Phys. Rev. A*, 2011, **84**, 053818.
- ²² T. V. Tscherbul and P. Brumer, *Phys. Rev. Lett.*, 2014, **113**, 113601–1–113601–4.
- ²³ T. V. Tscherbul and P. Brumer, *J. Chem. Phys.*, 2015, **142**, 104107–1–104107–9.
- ²⁴ M. Kiffner, M. Macovei, J. Evers and C. H. Keitel, *Prog. Opt.*, 2005, **55**, 85–197.
- ²⁵ R. A. Mathies and J. Lugtenburg, *Handbook of Biological Physics, Volume 3: Molecular Mechanisms in Visual Transduction*, Elsevier Science Press, Eds. D. G. Stavenga, W. J. DeGrip and E. N. Pugh Jr. edn., 2000.
- ²⁶ O. Wang, R. W. Schoenlein, L. A. Peteanu, R. A. Mathies and C. V. Shank, *Science*, 1994, **266**, 422–424.
- ²⁷ J. E. Kim, M. J. Tauber and R. A. Mathies, *Biochemistry*, 2000, **40**, 13774–13778.
- ²⁸ S. Hahn and G. Stock, *J. Phys. Chem. B*, 2000, **104**, 1146–1149.
- ²⁹ S. Hahn and G. Stock, *Chem. Phys.*, 2000, **259**, 297–312.
- ³⁰ B. Balzer, S. Hahn and G. Stock, *Chem. Phys. Lett.*, 2003, **379**, 351–358.
- ³¹ B. Balzer and G. Stock, *Chem. Phys.*, 2005, **310**, 33–41.
- ³² M. O. Scully and M. S. Zubairy, *Quantum Optics*, Cambridge University Press, Cambridge, UK, 1997.
- ³³ C. Cohen-Tannoudji, J. Dupont-Roc and G. Grynberg, *Atom-Photon Interactions: Basic Processes and Applications*, Wiley-VCH, Weinheim, 2004.
- ³⁴ K. Hoki and P. Brumer, *Procedia Chem.*, 2011, **3**, 122–131.
- ³⁵ K. Bravaya, A. Bochenkova, A. Granovsky and A. Nemukhin, *J. Am. Chem. Soc.*, 2007, **129**, 13035–13042.
- ³⁶ H.-P. Breuer and F. Petruccione, *The Theory of Open Quantum Systems, Chap. 3.4*, Oxford

University Press, Oxford, UK, 2002.

- ³⁷ K. Blum, *Density Matrix Theory and Applications, Chapter 8*, Springer-Verlag, Berlin, Germany, 3rd edn., 2012.
- ³⁸ M. Schlosshauer, *Decoherence and the Quantum-to-Classical Transition*, Springer-Verlag, Berlin, Germany, 3rd edn., 2007.
- ³⁹ T. V. Tscherbul and P. Brumer, *J. Phys. Chem. A*, 2014, **108**, 3100–3111.
- ⁴⁰ S. Menon and G. S. Agarwal, *arXiv:quant-ph/9902021v1*, 1999.
- ⁴¹ M. V. G. Dutt, J. Cheng, B. Li, X. Xu, X. Li, P. R. Berman, D. G. Steel, A. S. Bracker, D. Gammon, S. E. Economou, R.-B. Liu and L. J. Sham, *Phys. Rev. Lett.*, 2005, **94**, 227403–1–227403–4.
- ⁴² M. Spanner, C. Arango and P. Brumer, *J. Chem. Phys.*, 2010, **133**, 151101–1–151101–3.
- ⁴³ L. A. Pachón and P. Brumer, *J. Chem. Phys.*, 2013, **139**, 164123–1–164123–9.
- ⁴⁴ L. A. Pachón, L. Yu and P. Brumer, *Faraday Discuss.*, 2013, **163**, 485–495.
- ⁴⁵ T. A. Grinev and P. Brumer, *to be published*, 2015.
- ⁴⁶ L. Seidner and W. Domcke, *Chem. Phys.*, 1994, **186**, 27–40.
- ⁴⁷ W. T. Pollard and R. A. Friesner, *J. Chem. Phys.*, 1994, **100**, 5054–5065.